ALKALI ACTIVATION OF DIFFERENT TYPE OF ASH AS A PRODUCTION OF COMBUSTION PROCESS

by

Miloš T. NENADOVIĆ [1*], ***Claudio FERONE*** [2], ***Ljiljana M. KLJAJEVIĆ*** [3], ***Miljana M. MIRKOVIĆ*** [3], ***Bratislav Ž. TODOROVIĆ*** [4], ***Ivana S. VUKANAC*** [5], ***and Snežana S. NENADOVIĆ*** [3]

[1]Laboratory for Atomic Physics, Vinča Institute of Nuclear Sciences,
National Institute of the Republic of Serbia, University of Belgrade, Belgrade, Serbia
[2]Dipartimento di Ingegneria, Centro Direzionale Universita di Napoli "Parthenope", Isola C4, Napoli, Italy
[3]Laboratory for Materials Sciences, Vinča Institute of Nuclear Sciences,
National Institute of the Republic of Serbia, University of Belgrade, Belgrade, Serbia
[4]Faculty of Technology Leskovac, University of Niš, Niš, Serbia
[5]Laboratory for Radiation and Environmental Protection, Vinča Institute of Nuclear Sciences,
National Institute of the Republic of Serbia, University of Belgrade, Belgrade, Serbia

Scientific paper
https://doi.org/10.2298/NTRP201120006N

Presented study deals with the final structure and radiological properties of different fly-ash based geopolymers. Lignite fly-ash (lignite Kolubara – Serbia) and wood fly ash were obtained in combustion process together with commercial fly-ash. Synthesis of the geopolymers was conducted by mixing fly-ash, sodium silicate solution, NaOH and water. The samples were strengthened 60 °C for 48 hours after staying at room temperature in covering mold for 24 hours. The X-ray diffraction, Fourier transform infrared and SAM measurements were conducted on the samples after 28 days of geopolymerization process. The X-ray diffraction measurements of lignite fly-ash samples show anhydrite as the main constituent, while wood fly-ash samples consist of calcite, albite and gypsum minerals. Besides determination of physicochemical properties, the aim of this study was radiological characterization of lignite fly-ash, wood fly-ash and the obtained geopolymer products. Activity concentration of ^{40}K and radionuclides from the ^{238}U and ^{232}Th decay series, in ash samples and fly-ash based geopolymers, were determined by means of gamma-ray spectrometry, and the absorbed dose rate, *D*, and the annual effective dose rate, *E*, were calculated in accordance with the UNSCEAR 2000 report.

Key words: fly-ash, lignite, wood, geopolymerization, radionuclide

INTRODUCTION

Ashes, derived from the combustion process of solid or liquid fuels in power plants, consist predominantly of inorganic material and small portions of organics due to incomplete combustion. The composition of ash is strongly dependent on the fuel from which it is derived, the combustion technique and the combustion process control. Hence, ash compositions vary over a wide range. The most important development in the field of coal combustion products utilization in Europe, in 2004, was the approval of a revised European standard on fly-ash (FA) for concrete [1-8]. The standard covers siliceous FA and includes, for the first time, FA obtained from co-combustion of coal and certain co-combustion materials. The new standard introduces a quality control system for FA, consisting of an internal quality control by the producer and an audit testing by a certification body which is notified by the building authorities. The EU has approved the use of FA derived from the co-combustion of coal with wood, straw, olive husks, green wood, cultivated biomass, animal meal, municipal solid waste, and paper sludge as a cement admixture, as long as the FA contains less than 5 wt.% carbon, 5 wt.% total alkali, and 0.1 wt.% chloride [7-15]. Finding means of utilizing waste products is a very important and actual field of research. The FA, obtained as waste products, from different sources (wood and lignite) were used as a basic ingredient of the new geopolymeric materials [9]. The technology of geopolymerisation is gaining commercial interest because it has been demonstrated that, in certain cases, the properties of geopolymeric materials are superior to existing cementations systems [10]. Source materials used

* Corresponding author; e-mail: milosn@vin.bg.ac.rs

for the synthesis of geopolymers from by-products such as fly ash have an important role in determining the final properties of the geopolymer matrix [11]. van Jaarsveld *et al*. [2] has shown that the particle size, calcium content, alkali metal content, amorphous content, as well as morphology and origin of the FA, greatly affect the properties that impart on both the initial synthesis mix, as well as the final product. Also, they concluded that a chemical dissolution test, XRF analysis, and infrared absorption spectrum, will provide almost all the necessary information to predict how a specific FA will behave when used as a starting material in geopolymer synthesis.

The goal of this research is investigation of structural and radiological properties of a different kind of FA as precursor of geopolymer materials as a construction material. This is particularly important in terms of environmental protection and application in the cement industry. In that context, FA should have good binding properties. Besides that, an additional advantage would be a very low content of radionuclides and heavy metals, in order to minimize impact on the environment, as well as to provide safe wide consumption in civil engineering. In the process of burning a smaller portion of radionuclides deposited in the wood and lignite, evaporates and goes to atmosphere, while a larger portion is retained in the ash. The results of natural radionuclides ^{40}K, ^{232}Th, and ^{238}U (^{226}Ra), as well as of artificial radionuclide ^{137}Cs content determination in the ash, remained after burning the wood and lignite, are presented in this paper.

MATERIALS AND METHODS

Geopolymer samples were prepared starting from different FA precursors (FA- Class F coal FA (EFA-Fluler® HP) purchased from Baumineral (Germany), indicated from this point onward as FA; WFA-Wood FA and LFA-lignite FA) and by using sodium silicate solutions characterized by $R = 3.3$, provided by Prochin Italia Srl (Italy) and sodium silicate 1.5 (Serbia). Reagent grade NaOH was purchased by Aldrich. After mixing, samples have been poured in molds closed to avoid water evaporation and stored at 25 °C for 28 days. Table 1 shows the chemical composition of FA, GPFA-geopolymer from FA, LFA-lignite FA, GPLFA-geopolymer from lignite FA, WFA-wood FA, and GPWFA-geopolymer from wood FA samples, as determined by XRF analysis carried out by Bruker Explorer S4 apparatus.

The X-ray powder diffraction results were collected using Rigaku Ultima IV diffractometer, with CuK$\alpha_{1,2}$ radiation, with generator voltage 40.0 kV and generator current 40.0 mA. The range of 5°-80° 2θ was used for all powders in a continuous scan mode with a scanning step size of 0.02° at scan rate of 2 ° per minute. Mineralogical phase identification of all samples were done using PDXL2 software (version 2.8.30.) [16]. The ICDD database was used for phase identification [17].

Table 1. Chemical composition expressed in oxide of used precursors

WT.%	FA	GPFA	LFA	GPLFA	WFA	GPWFA
SiO_2	48.59	46.2	29.2	18.5	1.6	13.0
Na_2O	1.06	13.5	0.2	33.4	–	38.8
Al_2O_3	21.71	17.5	20.0	5.7	0.8	0.2
C		8.9	9.9	8.9	–	–
CaO	7.32	5.8	19.2	11.2	78.1	36.4
Fe_2O_3	8.03	3.5	7.8	3.2	–	–
K_2O	2.11	1.4	0.6	0.2	12.8	7.1
MgO	2.40	1.4	5.1	2.2	3.6	1.2
SO_3		1.3	7.6	16.4	0.7	1.3
TiO_2		0.6	0.4	0.2	–	–
P_2O_5					1.5	0.7
Mn_2O_3					0.9	1.3

Fourier-transform infrared spectroscopy (FTIR) analysis was used to monitor the forming of new chemical bonds during the synthesis. The functional groups of all the samples were studied using FTIR spectroscopy. Samples were powdered finely and dispersed evenly in anhydrous potassium bromide (KBr) pellets (1.5 mg/150 mg KBr). Spectra were taken at room temperature using a Bomem (Hartmann & Braun) MB-100 spectrometer set to give under formed spectra. The spectral data of the samples were collected in 4000-400 cm^{-1} region. The micro-structure analysis of the obtained GP materials was performed using a JEOL JSM 6390 LV electron microscope at 25 kV. The samples were previously Au coated in order to avoid charging problems.

Activities of naturally occurring radionuclides (^{226}Ra, ^{232}Th, and ^{40}K) were determined by means of gamma spectrometry in all the investigated samples. Powdered samples, prepared in the manner described in previous chapters, were placed in PVC cylindrical containers (125 ml), sealed and left for six weeks in order to reach radioactive equilibrium. Radiological analysis was performed by means of a coaxial semiconductor high purity germanium (HPGe) detector (Canberra GC5019, with 50 % relative efficiency and 1.8 keV resolution for ^{60}Co at the 1332 keV line) associated with standard beam supply electronics units. Certified solution of mixed gamma-emitting radio- nuclides (^{241}Am, ^{109}Cd, ^{139}Ce, ^{57}Co, ^{60}Co, ^{137}Cs, ^{113}Sn, ^{85}Sr, ^{51}Cr, ^{210}Pb, and ^{88}Y), purchased from the Czech Metrology Institute (CMI), was used for the preparation of standards for the energy and efficiency calibration of the spectrometer in accordance with IAEA recommendations [18]. All the spectra were recorded and analyzed using the Canberra's Genie 2000 software. Net areas of the peaks were corrected for the background, dead time and coincidence summing effects [19]. Obtained efficiencies were corrected for coincidence summing effect using

Table 2. Activity concentration of natural radionuclides in the investigated samples with associated measurement uncertainties ($k = 1$). Calculated radium equivalent activity, external radiation hazard index, external absorbed dose rate and annual effective dose rate

Samples	^{226}Ra [Bqkg^{-1}]	^{232}Th (^{228}Ac) [Bqkg^{-1}]	^{40}K [Bqkg^{-1}]	Ra_{eq} [Bqkg^{-1}]	H_{ex} [Bqkg^{-1}]	D [nGyh^{-1}]	EDR [mSv]
FA	217 7	84.8 3.2	506 17	377.23	1.02	172.57	0.21
GPFA	137 9	58.4 1.6	375 13	249.39	0.67	114.21	0.14
WFA	35 4	26 5	4000 200	380.18	1.03	198.67	0.24
GPWFA	13 1	18 2	1520 90	155.78	0.42	80.26	0.10
LFA	180 10	140 10	180 20	394.06	1.06	175.23	0.21
GPLFA	75 5	83 6	66 6	198.77	0.54	87.53	0.11

the correction factors obtained with EFTRAN software [19]. The measurement times were 60 000 seconds. The obtained specific activities are given in tab. 2, expressed in Bqkg^{-1}. Quoted uncertainties (the confidence level of 1) were calculated by error propagation calculation. The combined standard uncertainties included the statistical uncertainties of the recorded peaks, efficiency calibration uncertainty and the uncertainty of used correction factors.

Absorbed gamma dose rate

The external absorbed dose rate [nGyh^{-1}] outdoor at 1 m above the ground level was calculated using the equation

$$D \quad 0.462A_{\mathrm{Ra}} \quad 0.604A_{\mathrm{Th}} \quad 0.0417A_{\mathrm{K}} \qquad (2)$$

where the indexes: 0.462, 0.604, and 0.0417 are the dose conversion factors for ^{226}Ra, ^{232}Th, and ^{40}K, respectively, in soil [nGyh^{-1}/(Bqkg^{-1})] [20], and A_{Ra}, A_{Th} and A_{K} are the activity concentrations [Bqkg^{-1}] of ^{226}Ra, ^{232}Th, and ^{40}K.

Annual outdoor effective dose

In order to estimate the health effects of the absorbed dose, the annual effective dose (EDR) should be determined considering the conversion coefficients from the absorbed dose in air to the effective dose (0.7 SvGy^{-1}) and the outdoor occupancy factor (the fraction of time spent outdoors) of 0.2 both proposed by The United Nations Scientific Committee on the Effects of Atomic Radiation (UNSCEAR). The annual effective dose in units of mSv was estimated using the [11]

$$EDR\,[\mathrm{mSv}] \quad 10^{\ 6} \ D \ N_{\mathrm{h}} \quad 0.2 \ 0.7 \qquad (2)$$

where D is the absorbed gamma dose rate in air [nGyh^{-1}] and N_{h} – the annual exposure time (8760 hours).

External radiation hazard index and radium equivalent activity

The external radiation hazard index, H_{ex} and radium equivalent activity, Ra_{eq} are used to estimate the external radiation hazard due to the emitted gamma radiation. It was calculated according to the [20]

$$H_{\mathrm{ex}} \quad A_{\mathrm{Ra}} / 370 \quad A_{\mathrm{Th}} / 259 \quad A_{\mathrm{K}} / 4810$$
$$Ra_{\mathrm{eq}} \quad A_{\mathrm{Ra}} \quad 1.43A_{\mathrm{Th}} \quad 0.077A_{\mathrm{K}} \qquad (3)$$

The value of this index must be less than unity to keep the radiation hazard insignificant, *i. e.*, to keep the radium equivalent activity and annual dose under the permissible limits of 370 Bqkg^{-1} and 1 mSv, respectively.

RESULTS AND DISCUSSION

The X-ray diffraction

Figure 1 shows the X-ray diffraction (XRD) patterns of the FA, lignite FA (LFA), wood FA (WFA), and geopolymers (GPFA, GPLFA, and GPWFA).

As fig. 1(a) shows, the diffraction of most peaks from samples FA and GPFA belong to mullite and hematite while quartz peaks have considerably less frequency.

Higher background indicates the most likely presence of amorphous carbonaceous matter in the samples. It is important to note that in the second sample (GFA), mullite peaks have lower intensities than in the sample FA. The Fe_2O_3 phase is noted on diffractograms like H, but the positions of the peaks correspond more to maghemite (Fe_2O_3), which is a metastable phase with the respect to hematite with spinal-like structure, with cubic sub cell. As fig. 1(b) shows, powder diffraction patterns of samples LFA and GFLA. Based on the results of starting raw lignite material, it is evident that mineralogical composition corresponds to anhydrite as the most common phase. Diopside, calcium carbide, and kaolinite-montmorillonite type of clay is also found in PL sample. The mineralogical composition of obtained GFL sample is cor-

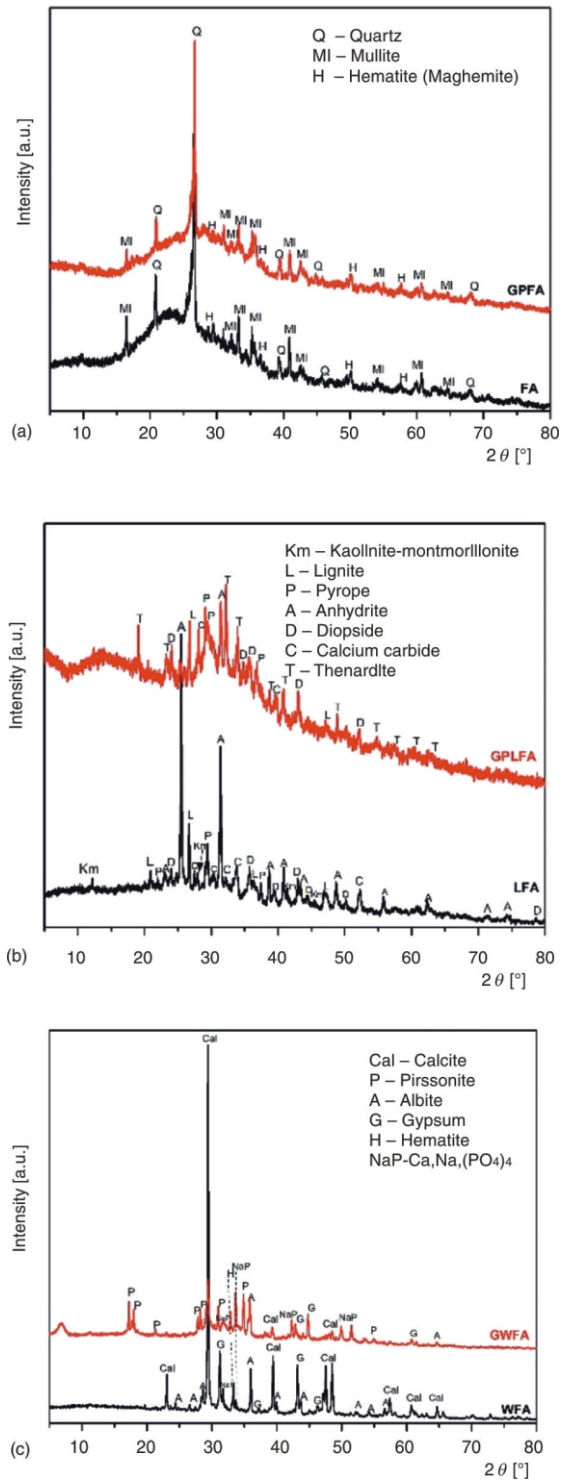

Figure 1. Powder diffraction pattern of samples: (a) FA and GPFA, (b) LFA and GPLFA, and (c) WFA and GPWFA

related with the sampling site Kolubara, Serbia. During geopolymer synthesis LFA-GLFA based on presented results, it is evident that anhydrite transforms to thenardite. The chemical composition anhydrite is $CaSO_4$ while the thenardite is Na_2SO_4 [20, 21]. Sample GLFA is mainly composed of thenardite which leads to conclusion that Na^+ from an alkaline solution during formation of geopolymer changes the Ca^{2+} from the structure of anhydrite dissolution and leads to the formation of thenardite as the ending phase [22]. Higher background and base line of GLFA sample indicate the achievement of amorphization during the geopolymerization process. As can be observed at fig. 1(c) the WFA sample consists mainly of calcite, albite and gypsum minerals. Due to geopolymerization process in highly alkaline environment it is evident that sample GWFA consists mainly of pirssonite ($Na_2Ca(CO_3)_2 \cdot 2H_2O$), which is most likely produced by the incorporation of sodium ions into the crystalline calcite structure [23-25]. Narrow and well -defined peaks of calcite, pirssonite and gypsum are present in both samples, which indicates a good structural arrangement of raw material and geopolymer.

Fourier-transform infrared spectroscopy analysis

The results of the FTIR analysis of the studied samples are presented in fig. 2. The FTIR absorption spectra were compared to known absorption lines in literature. The IR spectra were recorded in the spectral region 400 to 4000 cm^{-1}.

Figure 2(a) shows the FTIR spectra of the Class F coal FA, labeled as FA and geopolymer samples obtained by alkali activation of FA (GFA). The bands around 3450 and 1645 cm^{-1}, due to vibrations of hydroxyl groups, are observed. In the high-frequency (1200-650 cm^{-1}) region, the main band, centered at ~1040 cm^{-1}, is assigned to the Si(Al)-O-Si asymmetric stretch. This band is typical for the spectra of silicate glasses, and its frequency depends slightly on the state of hydration, NBO concentration and Al content [26, 27]. For the spectrum of quartz, the main Si-O stretching band is located at ~1050 cm^{-1} (overlapped with main band), with three relatively symmetric bands in the lower frequency: 793 cm^{-1}, 698 cm^{-1}, and 459 cm^{-1}. Comparing the spectra in fig. 1(a) (FA and GPFA), the intensity of the band near 1418, 1487, 1645 in sample GPFA -12 is much higher than in FA-12. Figure 2(b) shows the FTIR spectra of the wood FA and geopolymer samples obtained by alkali activation of WFA (GWFA). The signal at 1437 cm^{-1}, is attributed to the absorbance of carbonates [28]. The samples also showed absorbance of carbonates at 2518 cm^{-1} and 875 cm^{-1} [29-31]. In the GWFA, this signal is shifted to low wave number 1423 cm^{-1}. The typically most abundant elements in wood ash, Ca and K, were also among the most abundant elements in the FA. Typically, in wood ash obtained by simple combustion, Ca and K are found in the forms of carbonates and phosphates [28-30]. Figure 2(c) shows FTIR spectra of the lignite FA and geopolymer samples obtained by alkali activation of LFA (GLFA). Analysis of the FA by FTIR spectroscopy gave a very simple spectrum with signals at 1437 cm^{-1} and 875 cm^{-1} which are con-

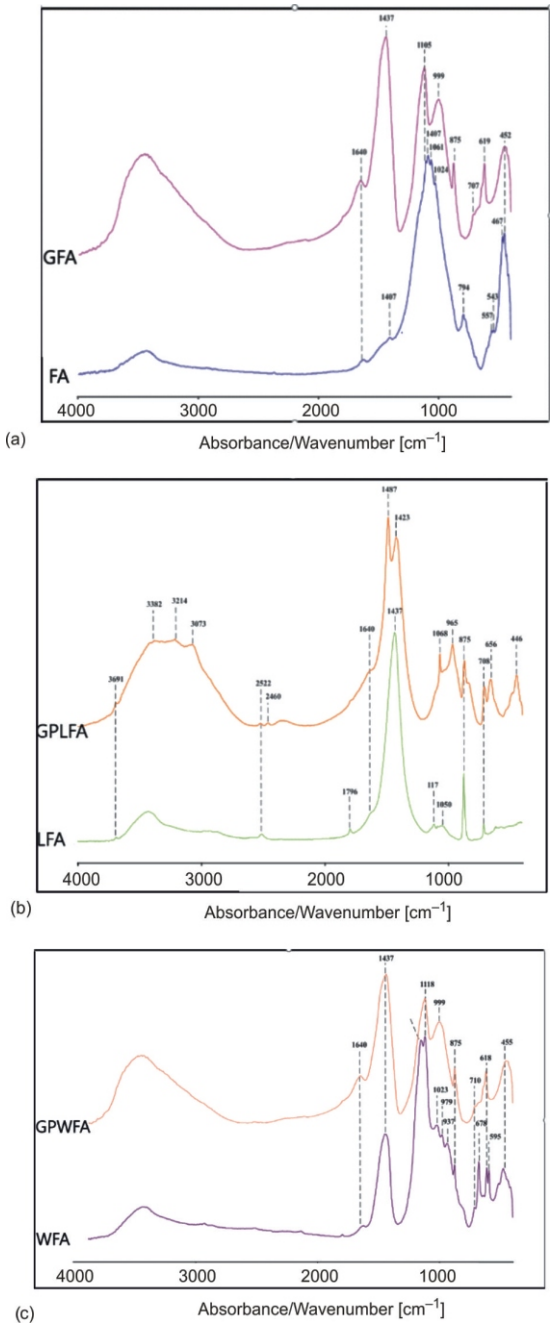

Figure 2. The FTIR spectra of: (a) FA and GFA, (b) LFA and GPLFA, and (c) WFA and GPWFA

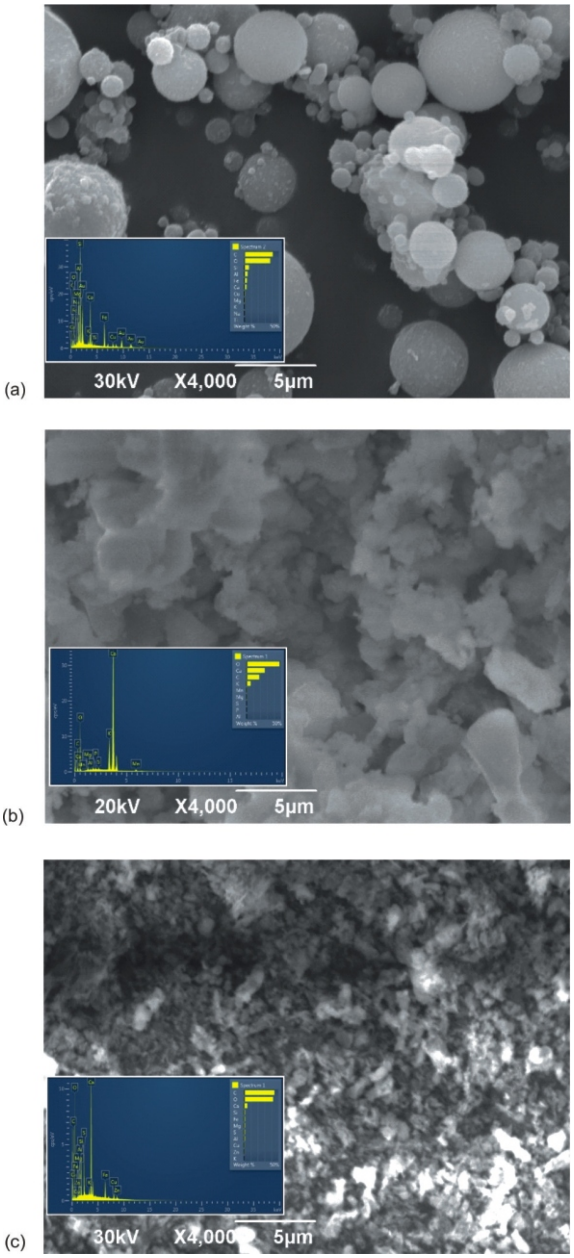

Figure 3. The SEM and EDS analysis: (a) FA, (b) WFA, and (c) LFA

sistent with the presence of carbonates fig. 2(a). After geopolymerization of the FA with alkali activator, these signals shifted to wave number 1423 cm^{-1} fig. 2(b).

Scaning electron microscope analysis

The SEM micrographs of precursors and them geopolymer samples are shown at figs. 3 and 4, respectively. In addition to the general physical characteristics and elemental composition of a random population of FA particles, the SEM data clearly indicated intermixing of Fe and Al-Si mineral phases and the predominance of Ca non-silicate minerals. These results supported data obtained from previous leaching studies and were consistent with XRD data. The morphology of a FA particle is controlled by combustion temperature and cooling rate. The sizes of the particles observed in this study ranged from less than 1 μm to greater than 5 μm. The majority of the particles ranged in size from approximately from 1 m to 3 μm and consisted of solid spheres fig. 3(a). Hollow cenospheres fig. 3(b) and irregularly shaped unburned carbon particles fig. 3(c) tended to be in the upper end of the size distribution.

Minerals and mineral aggregates, such as the quartz in fig. 4(a), often showed surface melting. Ag-

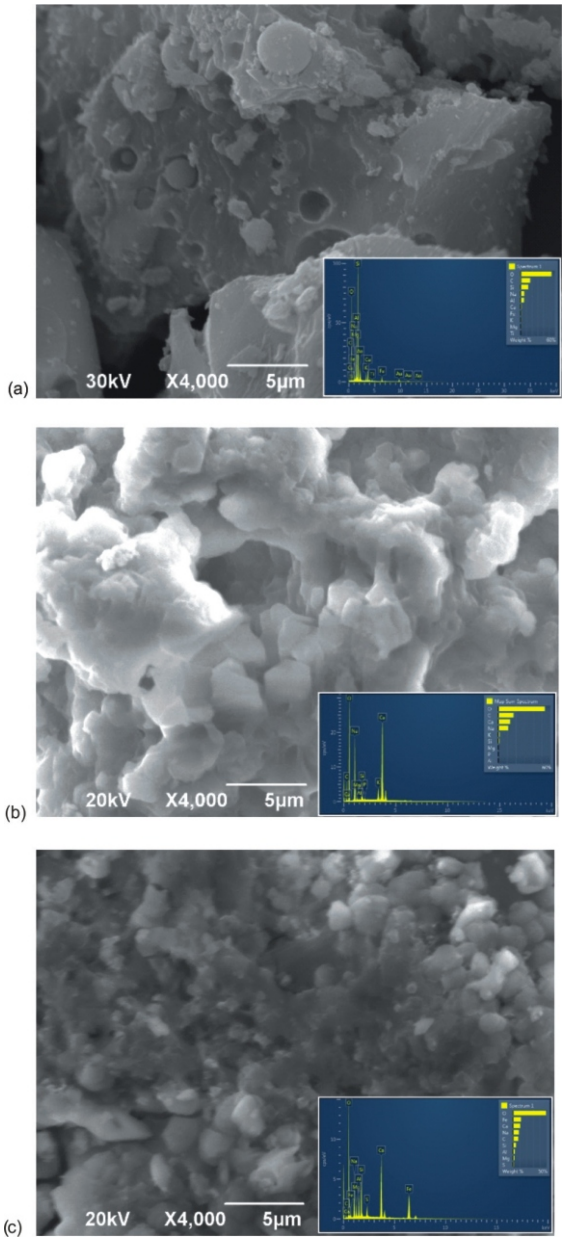

Figure 4. The SEM and EDS analysis: (a) GFA, (b) GWFA, and (c) GLFA

glomerated particles, fig. 4(b) and irregularly shaped amorphous particles fig. 4(c) may have been due to inter-particle contact or, rapid cooling. As determined by EDS, the predominant elements in the FA samples were silicon, aluminum, iron, calcium, and oxygen, in various compounds. Aluminum was primarily associated with silicon. Lesser amounts of the elements: potassium, magnesium, sodium, titanium, and sulfur, were observed with the aluminum and silicon. The only trace element identified was phosphorus and it was observed in only a few of the samples WFA and GPWFA. Calcium was observed primarily with sulfur or with phosphorus; it was not observed associated with silicon in any of the samples.

The FA samples consisted mostly of amorphous alumino-silicate spheres with a lesser number of iron-rich spheres. The majority of the iron-rich spheres consisted of two phases: an iron oxide mixed with amorphous alumino-silicate. This mixing of phases is consistent throughout the internal structure of the FA particles, not just a surface phenomenon. The amount of mixing varies with each FA particle, and several internal and surface textures were identified. The aluminum and silicon-rich spheres had minor elemental associations, similar to clay mineral matter.

Radiological analysis

Results of gamma spectrometric analysis are given in tab. 2, and based on these values dose calculations were performed.

Artificial radionuclide ^{137}Cs was detected in low concentration in WFA and GWFA samples. Naturally occurring radionuclides ^{238}U, ^{235}U, ^{226}Ra, ^{232}Th, and ^{40}K were detected in the measured samples. Measured specific activities in the samples of FA do not differ significantly from the activities of similar samples. Specific activities should have shown the enhancement in the first stage, *i. e*. after the combustion process of coal, lignite and wood, so activity per unit mass is expected to be higher due to water loss [11]. Statistically significant decrease of specific activity was detected for ^{40}K, ^{232}Th, and ^{226}Ra in synthetized geopolymer obtained from all FA, but for uranium isotopes change in specific activity was not that consistent.

Table 2 presents the total values of the Ra_{eq}, H_{ex}, D, and annual effective dose EDR originated from flay ash precursors and geopolymer samples obtained from them. The highest values of calculated parameters were mainly observed for raw materials. For all the synthetized materials, values of calculated EDR were significantly lower and relative decrease was the highest for LFA and GPLFA samples. Thus, considering radiological characteristics, investigated materials could be recommended as a promising construction material or its components.

CONCLUSION

Polymerization process, when it comes to alkaline activation of FA, leaded to a decrease of measured radionuclide content in all the measured geopolymer. In accordance with the presented results, generally, activity concentration is lower per unit of mass of synthesized geopolymers than in row materials used for their production. The amorphous gel phase is the major factor in the mechanical properties of the alkali activated calcined product based geopolymers. If the resulting geopolymer is more amorphous, or if it has more amorphous gel phase, it is more compact. The FTIR and SEM -EDS analysis were applied for determination a polymeric Si-O-Al framework and microstructure of

the investigated samples, respectively. The largest part of the geopolymers structure is amorphous and glass-like. The present crystalline phases are unevenly distributed in the amorphous matrix. They can cause stresses and bursting within the matrix, and therefore the pathway for releasing radionuclides into the environment. Calcium was associated with oxygen, sulfur or phosphorous, not with silicon or aluminum. The calcium-rich material was distinct in both elemental composition and texture from the amorphous alumino-silicate spheres. It was clearly a non-silicate mineral possibly mullite, hematite and quartz, confirmed using XRD analysis.

ACKNOWLEDGMENT

This research was financially supported by the Ministry of Education, Science and Technological Development of the Republic of Serbia.

AUTHORS' CONTRIBUTIONS

All the authors analysedanalyzed and discussed the results. Samples were synthetized by S. S. Nenadović and Lj. M. Kljajević. The manuscript was written by M. T. Nenadović, XRD analysis performed by M. M. Mirković, FTIR analysis performed by B. Ž. Todorović, SEM-EDS analysis by C. Ferone. Radioactivity measurements were performed by I. S. Vukanac.

REFERENCES

[1] Johnson, A., *et al*., Characterization and Evaluation of Fly-ash from Co-Combustion of Lignite and Wood Pellets for use as Cement Admixture, *Fuel, 89* (2010), 10, pp. 3042-305
[2] Jaarsveld, van J. G. S., *et al*., The Characterisation of Source Materials in FA-Based Geopolymers, *Materials Letters, 57* (2003), 7, pp. 1272-1280
[3] Nenadović, S., *et al*., Physicochemical, Mineralogical and Radiological Properties of Red Mud Samples as Secondary Raw Materials, *Nucl Technol Radiat, 32* (2017), 3, pp. 261-266
[4] Bošković, I., *et al*., Radiological and Physicochemical Properties of Red Mud Based Geopolymers, *Nucl Technol Radiat, 33* (2018), 2, pp. 188-194
[5] Bošković, I., *et al*., Characterization of Red Mud/Metakaolin-Based Geopoymers, *Materials and Technology, 53* (2019), 3, pp. 341-348
[6] Kljajević, Lj., *et al*., Structural and Chemical Properties of Thermally Treated geopolymer Samples, *Ceramics International, 43* (2017), 9, pp. 6700-6708
[7] Nenadović, S., *et al*., Chemical, Physical and radioogical Evaluation of Raw Materials and Geopolymer for Building Application, *Journal Radioanal Nucl. Chem, 325*, 2, pp. 435-445
[8] Ivanović, M., *et al*., The Effect of the Concentration of Alkaline Activator and Aging Time on the Structure of metakaolin Based geopolymer, *Sci Sinter, 52* (2020), 2, pp. 219-229
[9] Nenadović, *et al*., Structure Analysis of geopolymers Synthesized from Clay Originated from Serbia, *Environ Earth Sci, 76* (2017), Jan., pp. 76-79
[10] Mladenović, N., *et al*., The Applications of New Inorganic Polymer for Adsorption Cadmium From Wasrw Water, *Inorg Organomet Polym Mater, 30* (2020), 2, pp. 554-563
[11] Ivanović, M., *et al*., Physicochemical and radiological Characterization of Kaolin and its polzmerization Products, *Constr Build Mater, 68* (2018), p. 330, e155
[12] Gulicovski, J., *et al*., Geopolymer/CeO_2 as Solid Electrolyte for IT-SOFC, *Polymers, 12* (2020), 1, p. 248
[13] Kljajević, Lj., *et al*., The Influence of Alumino-Silicate Matrix Composition on Surface Hydrophobic Properties, *Sci Sint, 51* (2018), 2, pp. 163-173
[14] Kljajević, Lj., *et al*., Structural and Electrical Properties of geopolymer Materials Based on Different Precursors (Kaolin, Bentonite and Diatomite), *Maced J Chem Chem. Eng., 38* (2019), 2, pp. 283-292
[15] Nenadović, S. Lj., *et al*., Mechanochemical Treatment and Structural Properties of Lead Adsorption on Kaolinite (Rudovci, Serbia), *Environ Earth Sci, 73* (2015), 11, pp. 7669-7677
[16] Tokiy, R.C., PDXL Integrated X-Ray Powder Diffraction Softvare, 2011
[17] ***, (ICDD), I.C.f.D.D., Powder Doffraction File P-D, Announcement of New Database Release 2012, 2012
[18] ***, IAEA (1989) Measurement of Radionuclides in Food and the Environment, Technical Report Series No 295, Vienna, Austria
[19] Nikolić, J. T., *et al*., Calculation of HPGe Efficiency for Environmental Samples: Comparison of EFFTRAN and GEANT4, *Nuclear Instruments and Methods in Physics Research A, 763* (2014), Nov., pp. 347-353
[20] ***, UNSCEAR (2000) Sources and effects of ionizing radiation-United Nations Scientific Committe on the effects of Atomic Radiation, UNSCEAR 2000 Report to the General Assembly with Scientific Annexes, United Nations, New York
[21] Tchakoute, H. K., *et al*., Utilization of Sodium Water-Glass from Sugar Cane Bagasse Ash as a New Alternative Hardener for Producing Metakaolin-Based Geopolymer Cement, *Geochemistry, 77* (2017), 2, pp. 257-266
[22] Ossorio, M., *et al*., The Gypsum-Anhydrite Paradox Revisited, *Chemical Geology, 386* (2014), Oct., pp. 16-21
[23] Weidemann, H. G., Smykatz-Kloss, W., Thermal Studies on thenardite, *Thermochimica Acta, 50* (1981), 1-3, pp. 17-29
[24] Coudert, E., *et al*., Use of Alkali Activated High-Calcium FA Binder for Kaolin Clay Soil Stabilisation: Physicochemical Evolution, *Construction and Building Materials, 201* (2019), 5, pp. 539-552
[25] Avila-Lpoez, U., *et al*., Investigation of Novel Waste Glass and Limestone Binders Using Statistical Methods, *Construction and Building Materials, 82* (2015), May, pp. 296-303
[26] Abdel-Gawwad, H. A., A Novel Method to Produce Dry geopolymer Cement Powder, *HBRC Journal, 12* (2016), 1, pp. 13-24
[27] Taylor, W. R., Proc. Application of Infrared Spectroscopy to Studies of Silicate Glass Structure: Examples from the melilite Glasses and the Systems Na_2O-SiO_2 and Al_2O_3-SiO_2, *Indian Acad. Sci., (Earth and Planetary Science), 99* (1990), 1, pp. 99-117
[28] Gervais, F., *et al*., Infrared Reflectivity Spectroscopy of Silicate Glasses, *J. Non-Cryst. Solids, 89* (1987), 3, pp. 384-401

[29] Tatzber, M., *et al*., An Alternative Method to Measure Carbonate in Soils by FT-IR Spectroscopy, *Environmental Chemistry Letters, 5* (2007), 1, pp. 9-12
[30] Misra, M. K., *et al*., Wood Ash Composition Asa Function of Furnace Temperature, *Biomass Bioenerg, 4* (1993), 2, pp. 103-116
[31] Eberhardta, T. L., Pan, H., Analysis of the FA from the Processing of Wood Chipsin a Pilot-Scale Downdraft gasifier, Comparison of Inorganic Constituents Determined by PIXE and ICP-AES, *Biomass and Bioenergy, 51* (2013), Apr., pp. 163-168

Received on November 20, 2021
Accepted on April 7, 2021

Милош Т. НЕНАДОВИЋ, Клаудио ФЕРОНЕ, Љиљана М. КЉАЈЕВИЋ, Миљана М. МИРКОВИЋ, Братислав Ж. ТОДОРОВИЋ, Ивана С. ВУКАНАЦ, Снежана С. НЕНАДОВИЋ

АЛКАЛНА АКТИВАЦИЈА РАЗЛИЧИТИХ ВРСТА ПЕПЕЛА КАО ПРОИЗВОДА ПРОЦЕСА САГОРЕВАЊА

У раду су приказани структура и радиолошка својства различитих геополимера на бази летећег пепела. Лигнитни летећи пепео (лигнит Колубара – Србија) и дрвени летећи пепео добијени су у процесу сагоревања уз коришћење комерцијалног летећег пепела. Синтеза геополимера изведена је мешањем летећег пепела, раствора натријум силиката, NaOH и воде. Узорци су очвршћавани на 60 °C током 48 сати након задржавања на собној температури у покривајућем калупу током 24 сата. Мерења дифракције X-зрака, Фуријеове инфрацрвене трансформације и скенирајућег електронског микроскопа, извршена су на узорцима након 28 дана процеса геополимеризације. Рендгенска дифракциона мерења узорака лигнитног летећег пепела показују да је анхидрит главни састојак, док се узорци дрвеног летећег пепела састоје од минерала калцита, албита и гипса. Поред утврђивања физичко-хемијских својстава, циљ овог истраживања био је и радиолошка карактеризација лигнитног и дрвеног пепела, као и добијених производа геополимера. Концентрација активности ^{40}K и радионуклида из уранове (^{238}U) и торијумове (^{232}Th) серије у узорцима пепела и геополимерима на бази летећег пепела одређена је помоћу гама спектрометрије, а израчуната је јачина апсорбоване дозе D и годишња ефективна доза E у складу са извештајем UNSCEAR 2000.

Кључне речи: летећи пепео, лигнит, дрво, геополимеризација, радионуклид